Multi-layered nanoscale cellulose/$CuInS_2$ sandwich type thin films

Michael Weißl[1], Thomas Rath*[2], Jürgen Sattelkow[3], Harald Plank[3], Samuel Eyley[4], Wim Thielemans[4], Gregor Trimmel[2] and Stefan Spirk*[1]

1) Graz University of Technology, Institute of Paper, Pulp and Fibre Technology, Inffeldgasse 23A 8010 Graz

2) Graz University of Technology, Institute for Chemistry and Technology of Materials, NAWI Graz, Stremayrgasse 9 8020 Graz

3) Graz University of Technology and Centre for Electron Microscopy; Institute for Electron Microscopy and Nanoanalysis, Steyrergasse 17, 8010 Graz, Austria

4) Renewable Materials and Nanotechnology Research Group, Department of Chemical Engineering, KU Leuven Campus Kulak Kortrijk, Etienne Sabbelaan 53, 8500 Kortrijk, Belgium.

Correspondence:

Stefan Spirk

stefan.spirk@tugraz.at

+43 (316) 873 – 30763

Abstract

A generic procedure for the manufacturing of cellulose-metal sulfide multilayered sandwich type thin films is demonstrated at the example of copper indium sulfide. These multilayers were created by alternate spin coating steps of precursors, followed by their conversion using either acidic vapors, or heat treatment. As precursors, cellulose xanthate, a widely available cellulose derivative employed in viscose fiber manufacturing and commercial copper and indium xanthates were used. After conversion of the single layers into cellulose and copper indium sulfide, the film properties (structure, thickness, photoelectric activity) of the single and multilayer systems consisting of alternate layers of cellulose and copper indium sulfide were studied. For the proof of concept, up to five layers were built up, showing a clear separation of the cellulose and the metal sulfide layers as demonstrated using cross sectional analysis using ion slope beam cutting and SEM imaging. Finally, the conversion of xanthates was performed using UV light and a mask, allowing for the creation of 2D patterns.

Keywords

Cellulose xanthate, cellulose thin films, copper indium sulfide, metal xanthates, multilayer systems

Table of Content entry

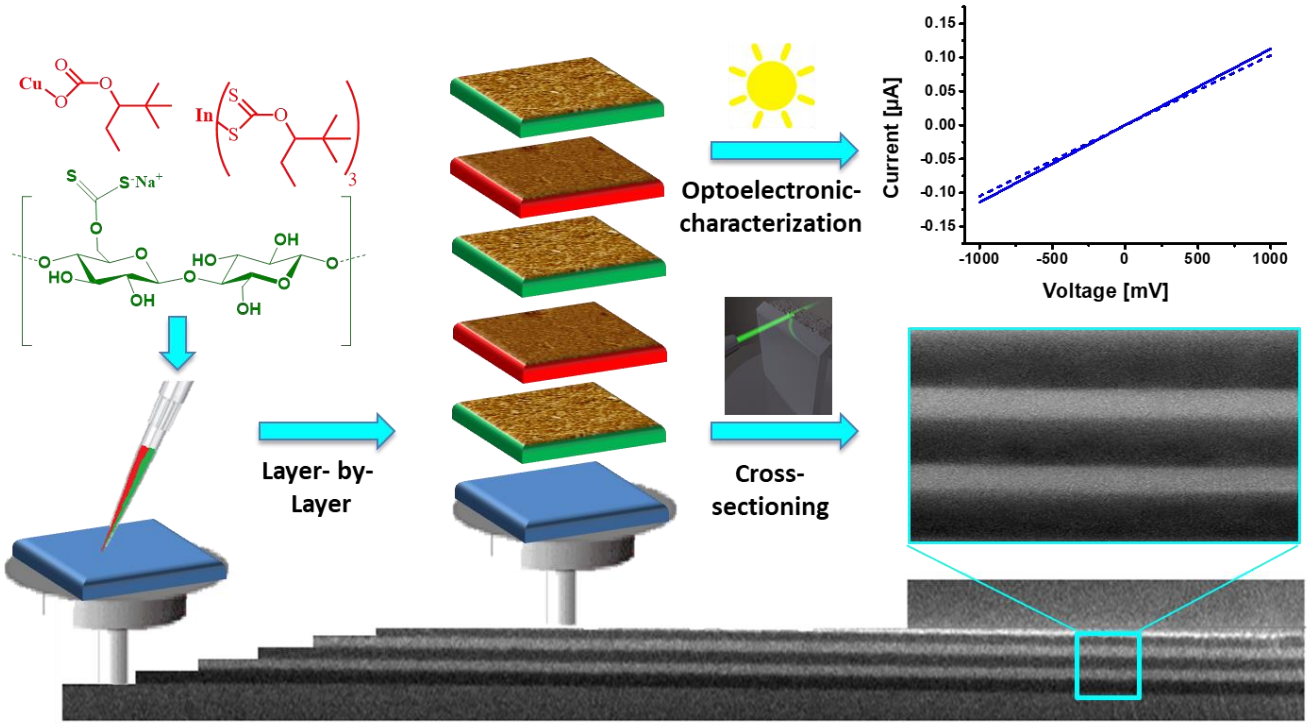

1. Introduction

Amorphous nanometric thin films of cellulose consist of randomly oriented chains with hardly any long range order.(E. Kontturi, Tammelin, & Österberg, 2006) Such materials offer a wide range of opportunities in understanding cellulose interaction with a variety of biomolecules(Filpponen et al., 2012; Kargl et al., 2013; K. S. Kontturi, Tammelin, Johansson, & Stenius, 2008; Mohan et al., 2013; Niegelhell et al., 2016; Orelma, Johansson, Filpponen, Rojas, & Laine, 2012) as well as water(Mohan et al., 2012) and they represent versatile substrates for functional layers in advanced materials such as optoelectronic devices.(Reishofer, Rath, et al., 2017; Wolfberger et al., 2015) Although one might expect that direct dissolution of cellulose and subsequent processing e.g. by spin coating can be used to produce such homogeneous nanometric films, problems associated with complete removal of solvents, homogeneous surface morphology and adhesion of the films on the substrate during regeneration impedes investigations of thin films manufactured via this route for such advanced applications. A different approach employs cellulose derivatives as starting materials which are converted back to cellulose after the processing step. In this context, the major material that has been used for the preparation of nanometric cellulose films is trimethylsilyl cellulose (TMSC).(Eero Kontturi, Thüne, & Niemantsverdriet, 2003; Schaub, Wenz, Wegner, Stein, & Klemm, 1993) TMSC can be dissolved in various organic solvents (depending on its degree of substitution with silyl groups) and converted back to cellulose after the processing step, e.g. by exposure to acidic vapors. Featureless surface morphologies are obtained via this route with high reproducibility. However, a major challenge of TMSC is, though commercially available in kg scale, that it is still rather expensive (several thousands of Euros/kg) and its production is difficult to upscale. Further, the use of water based systems for the creation of cellulose thin films would be desired. A potential solution to this challenge is the use of water soluble cellulose derivatives, which in addition

should be already produced in large scale. Cellulose xanthate (CX) is such a large scale, low cost commodity which is used in the viscose process for fiber/film formation. It is produced by alkali treatment of pulps (to remove low molecular weight components and homogenize molar mass distribution), followed by reaction with CS_2 to form CX. This solution is then subjected to ripening, where the xanthation pattern along the cellulose chains is significantly altered, leading to preferred substitution at C6. Afterwards, the material can be further processed to fibers and films. CX can be easily dissolved in aqueous NaOH in high concentrations and its properties in thin film formation can be tuned by variation of viscosity as shown recently.(Weißl et al., 2018) A potential limitation is that the regeneration of the xanthate to cellulose leads to the formation of sulfur containing products. However, in modern viscose manufacturing sites, the recycling rate of these products is larger than 99%, thereby not causing any significant negative impact for the environment. In addition, there are many processes in industry where sulfur containing compounds are released anyhow during the creation of new materials or compounds such as metal sulfides. Metal sulfides provide a wealth of properties whereas those with low band gap are particularly interesting for the creation of photoactive systems for optoelectronics.(Lai, Lu, & Chen, 2012) One potential route to manufacture such metal sulfides is the so called xanthate route, where a metal xanthate precursor is processed and by simple thermal treatment decomposition of the xanthate followed by the formation of the metal sulfides occurs.(MacLachlan et al., 2015; Macreadie Lauren, Maynard-Casely Helen, Batten Stuart, Turner David, & Chesman Anthony, 2014; Vagvala, Pandey, Ogomi, Ma, & Hayase, 2015) The side products of the xanthate decomposition are volatile and leave the metal sulfide matrix during the annealing step. This route does not only work for simple binary metal sulfides but also for more complex ones such as $CuInS_2$, a widely studied material with low band gap and high photoactivity. For the formation of $CuInS_2$, a mixture of a copper and an indium xanthate needs

to be heated to temperatures between 160 and 200 °C.(Rath et al., 2011) This method is very convenient for the fabrication of $CuInS_2$ nanocrystals, thin films or the formation of $CuInS_2$ nanocrystals directly in polymer thin films or other organic matrices.(Al-Shakban et al., 2018; Dunst et al., 2014; MacLachlan et al., 2015; Thomas Rath et al., 2013) However, only a few reports aim at replacing synthetic polymers used in this context by renewable ones such as cellulose.(Reishofer, Ehmann, et al., 2017; Reishofer, Rath, et al., 2017) In addition, the creation of multilayers involving cellulose and $CuInS_2$ requires the development of a technology that is capable of reproducibly manufacturing a subsequent layer system with basically no defects. In this paper, we address this challenge by using xanthates as the precursors for the creation of sandwich type structures featuring alternate cellulose and $CuInS_2$ layers. We study their formation and characterize the multilayered systems using FIB – SEM for any defects. Finally, we study the (photo-)conductivity properties of the layers in sandwich type structures involving up to 5 layers and correlate the layer thickness and the type of deposition with the obtained electrical response.

2. Experimental

2.1 Materials

Cellulose xanthate (CX) solution (10 wt.%, gamma: 52, NaOH: 6%, degree of polymerization: 550) was kindly provided by Lenzing AG (Lenzing, Austria).

Copper and indium xanthates (copper O-2,2-dimethylpentan-3-yl dithiocarbonate, indium O-2,2-dimethylpentan-3-yl dithiocarbonate) (Figure S1, supporting information) were purchased from Aglycon GmbH where it was synthesized based on a published protocol.(Rath et al., 2011)

Sulfuric acid (95 wt.%) and chloroform were purchased from VWR Chemicals, trifluoroacetic acid (TFA), chlorobenzene and hydrogen peroxide (30 wt.%) from Sigma-Aldrich.

Silicon wafers from Siegert Wafers (Aachen, Germany, wafer thickness: 675 ± 25 µm, 1 cm x 2 cm), glass slides from Roth (Karlsruhe, Germany, thickness: 1000 µm, 1.5 cm x 1.5 cm), Au-coated glass slides from BioNavis (Tampere, Finland, gold layer thickness: 50 nm, 1 cm x 2 cm, SPR102-AU), Filter Chromafil Xtra PVDF-45/25 0.45 µm as well as a two-component conductive epoxy glue from Chemtronics (Kennesaw, USA) were used as obtained.

2.2 Multilayer preparation

As substrates for the multilayer films, single side polished silicon wafers, gold coated glass slides and glass slides were used. The slides were cleaned by dipping them into piranha acid (H_2SO_4:H_2O_2 = 3:1 (v/v)) for 30 minutes (10 minutes for gold slides) and intensely washed with MilliQ water (≥18 MΩcm^{-1}) afterwards.

For layers 1, 3 and 5 of the thin film stack, cellulose xanthate (80 µl per square centimeter of substrate) was deposited onto the surfaces and subjected to spin coating (a = 2500 rpm·s^{-1}, v = 4000 rpm, t = 60 s). Spin coating was followed by regeneration of the deposited CX layers in vaporous TFA atmosphere. For the regeneration procedure, the TFA was diluted (1:1, with deion. water), placed into a watchglass (2 mL), and the substrates were positioned above the liquid TFA phase with help of a petri dish. A crystalizing dish was used as a lid to close the system. After 20 minutes exposure to the gaseous TFA atmosphere, regeneration of the cellulose xanthates to cellulose is accomplished as proven by ATR-IR spectroscopy (Figure S2, supporting information). Afterwards, the films were rinsed twice with water (8 mL) followed by drying in a stream of dry nitrogen. This process has to be repeated for every single cellulose layer.

For the preparation of the nanocrystalline $CuInS_2$ layers, (Layer 2 and 4), a precursor solution (CuInX, in chlorobenzene) containing copper xanthate (32.2 mg mL^{-1}, 1 equiv., 0.126mmol L^{-1}) and indium xanthate (147.8 mg mL^{-1}, 1.7 equiv., 0.215 mmol L^{-1}) was prepared. This CuInX solution (20 µL per square centimeter of substrate) was transferred onto the substrate and subjected to spin coating (a = 1000 rpm·s-1, v = 1000 rpm, t = 60 s). After spin coating, the CuInX was exposed to 170°C for 15 minutes to generate the nanocrystalline $CuInS_2$ thin film by thermal decomposition of the metal xanthates. (Pradhan, Katz, & Efrima, 2003) The process steps have to be repeated for every $CuInS_2$ layer in the multilayer system.

For electrical characterization, the single $CuInS_2$ layers of the multilayer system were contacted with copper electrodes. For this, conductive two component epoxy glue was employed. After mixing the two components, a little spot was placed on the $CuInS_2$ surface and small copper stripes (15 mm x 3 mm) were fixed on the $CuInS_2$ layers via the small glue spots. To accelerate the solidification of the epoxy glue, the substrates were placed in a drying oven at 60°C for two hours. After fixing the electrodes on the $CuInS_2$ layers, the step wise multilayer development could be continued.

2.3 Optical microscopy

Light microscopy investigations were carried out on an Olympus BX60 microscope fitted with an Olympus E-520 camera.

2.4 Profilometry

The layer thickness was determined with a Bruker DekTak XT surface profiler. The scan length was set to 1000 µm over the time duration of 3 seconds with the hills and valleys scanning profile. The diamond stylus had a radius of 12.5 µm and the employed force was 3 mg. The

measured profile was then used to determine the thickness. Each layer thickness has been determined by averaging 10 measurements on three different slides.

2.5 Attenuated total reflection – infrared spectroscopy

The infrared spectra were recorded with an ALPHA FT-IR spectrometer (Bruker; Billerica, MA, U.S.A.). For the measurements, an attenuated total reflection (ATR) attachment was used with 64 scans at a resolution of 4 cm^{-1} and a scan range between 4000 and 400 cm^{-1}. The samples were prepared on Au-coated glass slides (SPR102-AU). The data were analyzed with OPUS 4.0 software.

2.6 XPS

Spectra were recorded on a Kratos Axis Supra X-ray Photoelectron Spectrometer employing a monochromatic Al Kα (hν = 1486.7 eV, 10 mA emission) X-ray source, hybrid (magnetic/electrostatic) optics with a slot aperture, hemispherical analyzer, multichannel plate and delay line detector (DLD) with a take-off angle of 90°. The analyzer was operated in fixed analyzer transmission (FAT) mode with survey scans taken with a pass energy of 80 eV and high resolution scans with a pass energy of 20 eV. Samples were electrically isolated from the instrument. All scans were acquired under charge neutralization conditions using a low energy electron gun within the field of the magnetic lens. The resulting spectra were processed using CasaXPS software. Binding energy was referenced to aliphatic carbon at 285.0 eV.

2.7 Atomic force microscopy

The multilayer system was characterized with a FastScanBio AFM operated by a Nanoscope V controller (Bruker NANO, Santa Barbara, CA). All studies were performed in tapping mode with a Fast Scan A (Bruker AFM Probes, Camarillo, CA) cantilever with spring constants of 18 N/m, resonance frequencies around 1.4 MHz and a nominal tip end radius of 5 nm. Sample roughness

for each layer was measured at least at 3 different areas. At each region, 10x10 µm overview and 1x1 µm detail scans for high resolution were conducted. Concomitantly, to establish soft-repulsive conditions throughout the AFM investigation scan rates, amplitude set points, and feedback gains were monitored steadily for artifact free imaging conditions and lowest possible energy dissipation. Data analysis was conducted in NanoScope Analysis 1.5 (Bruker, Santa Barbara, CA).

2.8 Ion Beam Slope Cutting and scanning electron microscopy

Ion beam slope cutting and scanning electron microscopy (SEM) were performed in a NOVA 200 dual beam instrument (Thermo Fischer). SEM imaging has been performed at 10 keV and 540 pA with shortest possible image acquisition times to minimize e-beam damage for the cellulose layers. Broad ion beam processing was performed with an ILION instrumentation (GATAN) using 4 keV and cooled sample stages.

For the cutting, the sample was fixed on a metal blade and exposed to a perpendicular oriented broad ion beam using Ar ions. The metal blade does not protect the sample itself (Figure S3, supporting information) but also ensures a flat cross cut after processing. To further minimize heating effects, the entire sample was cooled by liquid nitrogen to -160 °C. The resulting cross section was flat and thus well suited for SEM based imaging and elemental analysis.

2.9 Contact angle and surface free energy determination

For the calculation of the surface free energy (SFE) Milli-Q water (≥18 $M\Omega cm^{-1}$) and diiodomethane were employed as test liquids. The drop shape analysis was done in the sessile drop modus at 25 °C with a DSA100 system (Krüss GmbH, Hamburg, Germany) equipped with a T1E CCD video camera (25 fps). The dispense rate of the 3 µL droplets was adjusted to 166 µL/min and the time before the image was captured was set to 2 seconds. Each sample was measured at least three times. The contact angle (CA) calculations (software: DSA1 v 1.90) were

performed with the Young-Laplace equation and the surface free energy calculation with the Owens-Wendt-Rabel & Kaelble method.(Owens & Wendt, 1969)

2.10 UV-VIS spectroscopy

Transmission and reflection spectra were recorded on a Perkin Elmer LAMBDA 35 spectrophotometer equipped with a 50 mm integrating sphere attachment. Absorption spectra were calculated from the transmission and reflection spectra.

2.11 Electrical characterization

JV characteristics of the $CuInS_2$ thin films were recorded in a glovebox using a Keithley 2400 source measure unit and a custom made LabView software. The samples were illuminated by a Dedolight xenon lamp with a spectrum similar to the AM 1.5G spectrum at 100 mW cm^{-2}. The current was measured between -1000 mV and 1000 mV for both illuminated and non-illuminated samples. The distance between the two electrodes was set to 10 mm.

2.12 Micropatterning

Micro patterning of the $CuInS_2$ films by selective conversion of the precursor layers by UV light

CuInX was selectively converted to $CuInS_2$ by patterned exposure of the layers to UV light emitted from an Efos Novacure UV spot curing system N2001 (Ontario, Canada). The lamp was equipped with a radiometer to regulate light intensity. The samples were placed in a silica glass tube with their back side up, the UV source was placed directly below the samples on the outer side of the tube. Before starting illumination, with a power of 5000 mW for 20 minutes, the glass tube was evacuated. To get a defined micro structuring, thin photomasks with varying structures (1 cm x 1 cm) were placed above the CuInX layers. After UV treatment, the non-exposed areas of the CuInX precursor film were removed by rinsing with chloroform and the sample with the remaining $CuInS_2$ structures were placed on a heating plate to obtain full conversion to $CuInS_2$.

3. Results and discussion

The general strategy for the solution-based manufacturing of multilayered cellulose-$CuInS_2$ systems was to use xanthates as precursors for both the cellulose, and the $CuInS_2$ thin films. The idea is to alternatively spin coat the respective xanthates and to convert the precursor layers into cellulose or the metal sulfide by exposure to acid vapors (CX) or exposure to elevated temperatures (CuInX). By variation of the concentration of either the CX or the CuInX variations in film thickness can be obtained.

3.1 Regeneration

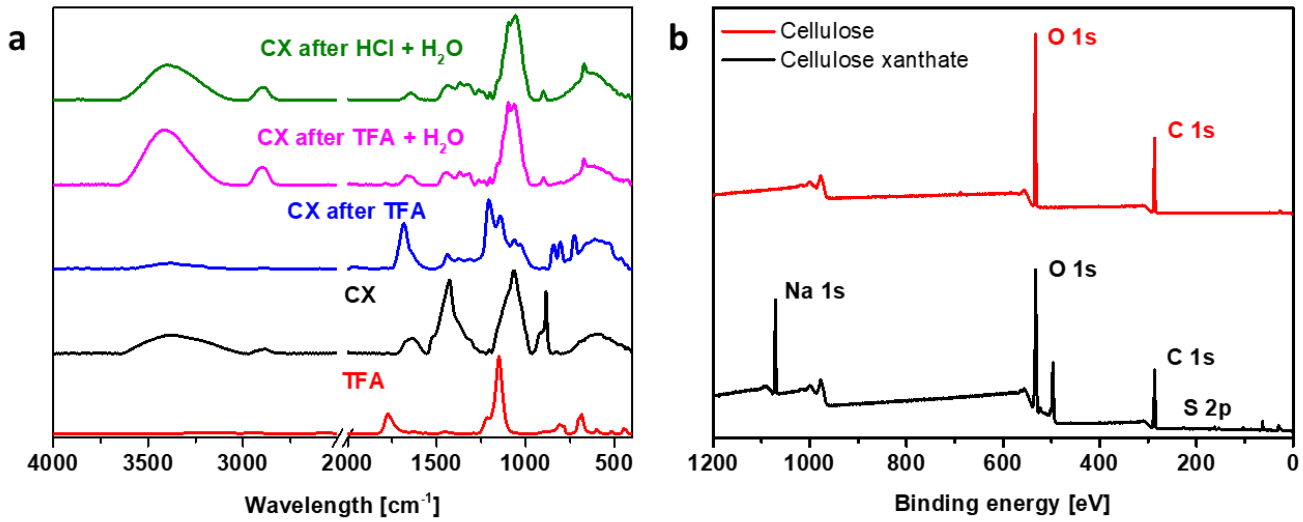

Figure 1. a) ATR-IR spectra of TFA, a CX film after spin coating and CX films after exposure of CX to HCl or TFA acidic atmosphere for 20 minutes followed by washing with deionized H_2O. b) XPS survey spectra of a CX film after spin coating and after the regeneration procedure.

Since HCl vapors are prone to attacking the $CuInS_2$ layers, trifluoroacetic acid (TFA) vapor was found to be the most promising alternative. A useful means to investigate the regeneration of cellulose xanthate is to employ ATR-IR spectroscopy and to follow the appearance and

disappearance of functional groups as a function of exposure to TFA vapors. TFA itself features characteristic bands at 1775 ($\nu_{C=O}$), 1624 (ν_{C-O}), 1460 cm^{-1} ($\nu_{C-O;}$ ν_{sC-O-C}) and two series of strong, overlapping bands from 1250 to 1100 cm^{-1} ($\nu_{CF3;}$ $\nu_{F-CF2;}$ $\nu_{F-C-F;}$ ν_{C-C}) and from 891 to 785 cm^{-1} ($\nu_{C-C;}$ ν_{C-O-O}) as well as strong bands at lower wave numbers, namely 660 cm^{-1} (δ_{CF3}); 600 cm^{-1} (δ_{F-CF2}), and 520 cm^{-1} (δ_{F-C-F}) corresponding to vibrations of the fluorinated carbon and carbon - carbon vibrations.(Redington & Lin, 1971; Spirk, Belaj, Kahr, & Pietschnig, 2009)

The spectra of the pure CX thin films indicate the partial regeneration of the films during the spin coating step as well as the presence of by-products in the CX solution. C=S and C-S vibrations have been reported in a range of 1250 – 1050 cm^{-1} for the CX and these bands interfere with decomposition products like sodium sulfide (1420, 920 cm^{-1}) or sodium trithiocarbonate (1670, 1427, 925 and 885 cm^{-1}). The remaining bands are caused by additional decomposition products such as CS_2 ($\nu_{C=S}$ at 1520 cm^{-1}) and, in traces, H_2S (ν_{S-H} at 2630 cm^{-1}) as well as NaOH (2725, 1452 and 1382 cm^{-1}).(Andrews, Hurtubise, & Krassig, 1960; Dautzenberg & Philipp, 1970; Ogura & Sobue, 1968) After exposure of the CX layers to acidic vapors of TFA, the spectrum changes significantly, and the bands corresponding to C=S, C-S or NaOH vibrations disappear. Instead, IR bands of two different species became visible, namely cellulose II bands and those ascribed for TFA-related compounds which are partially overlapping with the cellulose II bands. We have reported in a former study(Weißl et al., 2018) that sodium chloride is developed by deposition of CX layers in HCl vapor phase and in accordance to this, sodium trifluoroacetate (NaTFAA) is formed after TFA treatment. The bands related to vibrations of C=O, C-O, C-C and C-O-O (1684, 843, 725), are slightly shifted to lower wavenumbers compared to the TFA bands. In addition to the described NaTFAA bands, the bands at 3500 cm^{-1} - 3200 cm^{-1} (ν_{OH}), and from 1450 – 1310 cm^{-1} (C-O-H bending at 1430 cm^{-1}, C-H deformation at 1372 $cm^{-1}$and OH in plane

deformation at 1330 cm^{-1}) as well as a weak band at 900 cm^{-1} (C-O-C valence vibration) indicate the presence of cellulose II. After washing the samples with water, the bands associated to NaTFAA vanish and a characteristic cellulose II type spectrum (Figure 1a) is observed.(Široký, Blackburn, Bechtold, Taylor, & White, 2010) Finally, it should be noted here that immersion of the films in diluted solutions of TFA (which would eliminate the washing step to remove the salts) led to the peeling off the film from the substrate.

In addition to ATR-IR spectroscopy XPS was employed to validate the regeneration of the precursors (CX and CuInX) to cellulose and $CuInS_2$.

The cellulose xanthate film showed several sulfur environments. Based on the $S2p_{3/2}$ binding energy, the environment at 161.9 eV corresponds well to the two equivalent sulfur atoms of organic xanthates in the literature.(Mikhlin, Karacharov, & Likhatski, 2015) The second sulfur environment at 163.6 eV could be assigned to the extra sulfur atom present in trithiocarbonates, while the higher binding energy environments at 166.2 eV and 168.1 eV are typical of oxygen containing sulfur environments such as sulfoxides and sulfonates/sulfates (respectively). In the O1s spectrum, the lower binding energy environment at 531.3 eV corresponds well with metal salts of oxygen species and sulfates, while the higher binding energy environment at 533.0 eV corresponds with organic oxygen environments. Finally, the C1s spectrum contains four environments. Besides the usual aliphatic carbon (contamination) at 285.0 eV, there is C-O at 286.7 eV and O-C-O at 288.2 eV typical of cellulosic materials. The fourth environment with a binding energy of 289.4 eV is ascribed to xanthate due to the similarity in binding energy to urethanes, carbonates or ureas. After exposure to TFAA and rinsing with water, the sulfur containing bands disappear and a typical XPS spectrum of pure cellulose is obtained, with C1s and O1s contributions matching previously published data on cellulose thin films (Figure S4 a, supporting information).(Mohan et al., 2012)

High resolution spectra of the $CuInS_2$ layers showed that the binding energies of the $Cu2p_{3/2}$ and $In3d_{5/2}$ (932.3 and 445.0 eV) are in very good agreement with literature values (932.2 vs 444.7 eV) for $CuInS_2$ (Figure S4 b, supporting information).(T. Rath et al., 2013; Scheer & Lewerenz, 1994) The sulfur 2p spectrum confirmed the results from the Cu2p and In3d spectra, with binding energies for $S2p_{3/2}$ of 161.9 eV and $S2p_{1/2}$ of 163.0 eV characteristic for $CuInS_2$. The C1s spectrum of the $CuInS_2$ sample revealed a large amount of aliphatic carbon contamination (285.0 eV) with very small contributions due to C-X (O,S) species at 286.6 eV and O-C=O at 288.9 eV. These species correlate well with the O1s spectrum which shows three environments at 530 eV, 531.9 eV and 533.3 eV corresponding to metal oxides, and various carbon-oxygen species. The predominance of these latter two environments points to a relatively small amount of oxidation of the $CuInS_2$ layer with oxygen being confined to the organic contamination overlayer.

3.2 Multilayer architecture

After optimization of the regeneration of the CX, multilayer formation was studie. CX always was the very first layer deposited by spin coating onto the substrate. After conversion to cellulose by TFA vapor treatment, rinsing with water to remove NaTFAA, and drying in a stream of nitrogen, the CuInX solution was deposited by spin coating as well. The $CuInS_2$ film was created by heating the films on a heating plate at 170° for 15 minutes.(Fradler et al., 2014; Rath et al., 2011) After cooling, the procedure was repeated until five layers (cellulose - $CuInS_2$ – cellulose - $CuInS_2$ - cellulose) had been deposited onto the substrate. The development of the multilayer as well as the conversion of the CX into cellulose and the CuInX into $CuInS_2$ can be followed by ATR-IR spectroscopy since also the copper and indium xanthates feature characteristic bands. In Fig. 2 the IR spectra of a three-layered system (cellulose – $CuInS_2$ – cellulose) are shown.

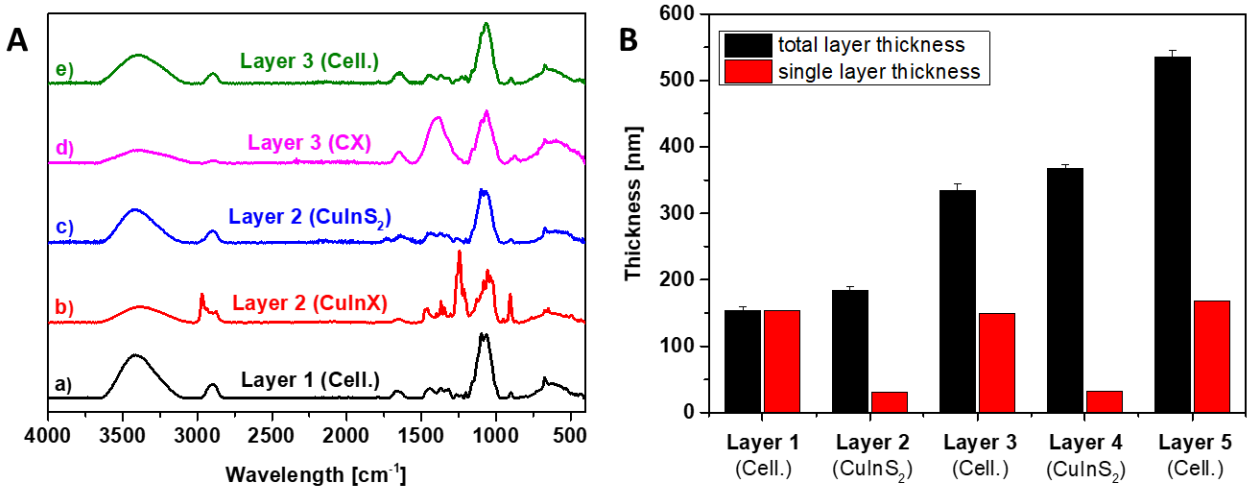

Figure 2. Left: ATR-IR spectra showing the development of a three-layered (cellulose – $CuInS_2$ – cellulose) multilayer system, starting with a fully processed cellulose layer(a), followed by the deposition and corresponding conversion of CuInX to $CuInS_2$ (b,c). The last two steps shown in the figure belong to the development of the third layer of the system, namely the deposition of CX and its regeneration to cellulose in TFA acidic atmosphere (d,e). Right: Development of the total film thicknesses and the individual layer thicknesses in a five layered cellulose $CuInS_2$ system.

The deposition of the CuInX onto the cellulose layer results in the appearance of new bands assignable to the bulky branched alkyl group of the CuInX in the region of 3000 to 2850 cm^{-1} (ν_{CH3}, ν_{CH2}, ν_{CH}) and strong bands at 1240 ($\nu_{C=S}$) and 1214 cm^{-1} (ν_{C-O-C}). After heat treatment, these bands disappear since the volatile side products leave the film while $CuInS_2$.was formed. The remaining two spectra in Figure 2 describe the deposition of another CX layer on the $CuInS_2$ and its conversion to the cellulose by exposure to TFA vapors.

For the 5 layered system, layer thicknesses of 154, 150 and 168 nm have been determined for the cellulose layers (L1, L3, L5), while for the $CuInS_2$ layers thicknesses of 30 (L2) and 32 nm (L4)

were determined (Figure 1) An overview on the layer thicknesses can be found in the SI (Table S1). The height profiles used for determination of the layer thickness revealed smooth surfaces without any major irregularities as shown in profilometry investigations.

3.3 Surface morphology and cross section analysis

To gain a more detailed topological information on the different layers in the cellulose $CuInS_2$ multilayer device, atomic force microscopy was employed (Fig. 3). When taking into consideration that there are already two more layers below, layer 3 (a cellulose layer) showed a rather flat surface, with a RMS roughness below 3 nm. The structure is regular and smooth over a large area and just a few agglomerates (height ca 10 nm) are visible. The surface after deposition of layer 4 ($CuInS_2$) changes, although the RMS roughness is in the same range. However, there is a certain influence of the layer 3; particularly the few aggregates can be clearly seen. A closer look onto the $CuInS_2$ layer illustrates that the $CuInS_2$ layer consists of spherical grains with the larger ones having diameters ranging from 20 to 30 nm.(Figure S5, supporting information) After deposition of the 5th layer and subsequent regeneration, a similar topography as for layer 3 was observed. Although the surface structure and roughness is a little smoother, compared to L3.

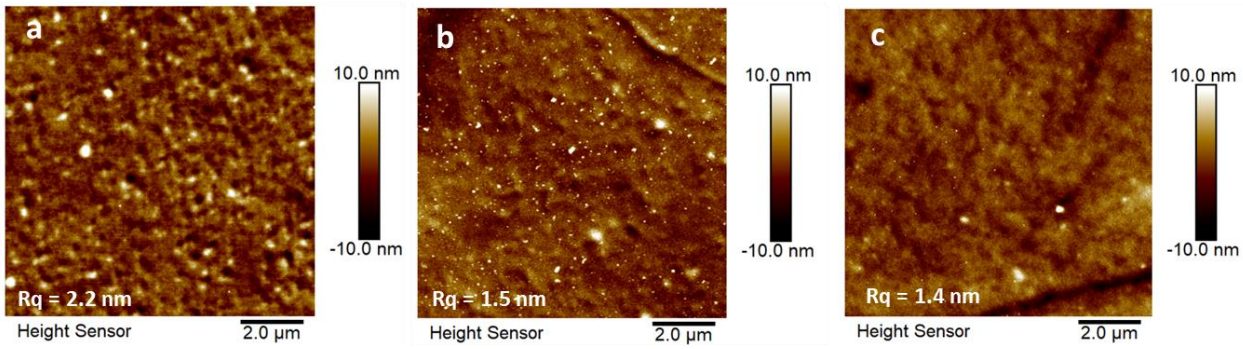

Figure 3. AFM topography images (10 x 10 µm²) after the final processing of Layer 3 (a), Layer 4 (b) and Layer 5 (c).

Although profilometry and AFM images suggest that the single layers are homogeneous and hence do not intermingle, only cross section images are capable to prove a full picture of the multilayer structure. However, a major problem in such investigations is the preparation of cross sections due to the following reasons. Cellulose is a sensitive material prone to decomposition in an ion/electron beam and, in addition, the multilayer consists of hard (Si-Wafer, $CuInS_2$) and soft (cellulose) layers making polishing, microtomy or FIB sectioning extremely challenging. For such samples, the favored option is probably to employ ion beam slope cutting. Here, a protective metal stripe is deposited on the surface of the layer and an Ar-beam is used to cut a slice of the layer, which can then be moved using micromanipulators to SEM imaging at the same time. Further, the sample needs to be cooled (-160 °C) in order to avoid any degradation of cellulose by the ion beam. Using this approach, we obtained high quality cross sectional images with hardly any beam damage of our samples. The cross sections (Fig. 4) images confirmed the results of the other analyses and a clear multilayer structure is observed. The layers feature a high degree of conformity, they show a constant thickness over a large area (i.e. 40 microns) and the different layers are clearly separated. These cross sections were employed for a more precise determination of the $CuInS_2$ layer thicknesses and more accurate data than with profilometry was obtained. The cellulose layers feature a layer thickness between 140 and 150 nm, while the $CuInS_2$ layers feature layer thicknesses of 45-50 nm. These layer thicknesses are a bit smaller than those determined by profilometry which is probably due to the slight shrinkage of the cellulose layers during heating as reported earlier.(Mohan et al., 2012) The thickness of the $CuInS_2$ layer can be easily tuned, for instance an increase in the CuInX concentration by a factor of 2 in the solution yielded final $CuInS_2$ layer thicknesses ranging from 90 to 100 nm (i.e. layer thickness doubled).

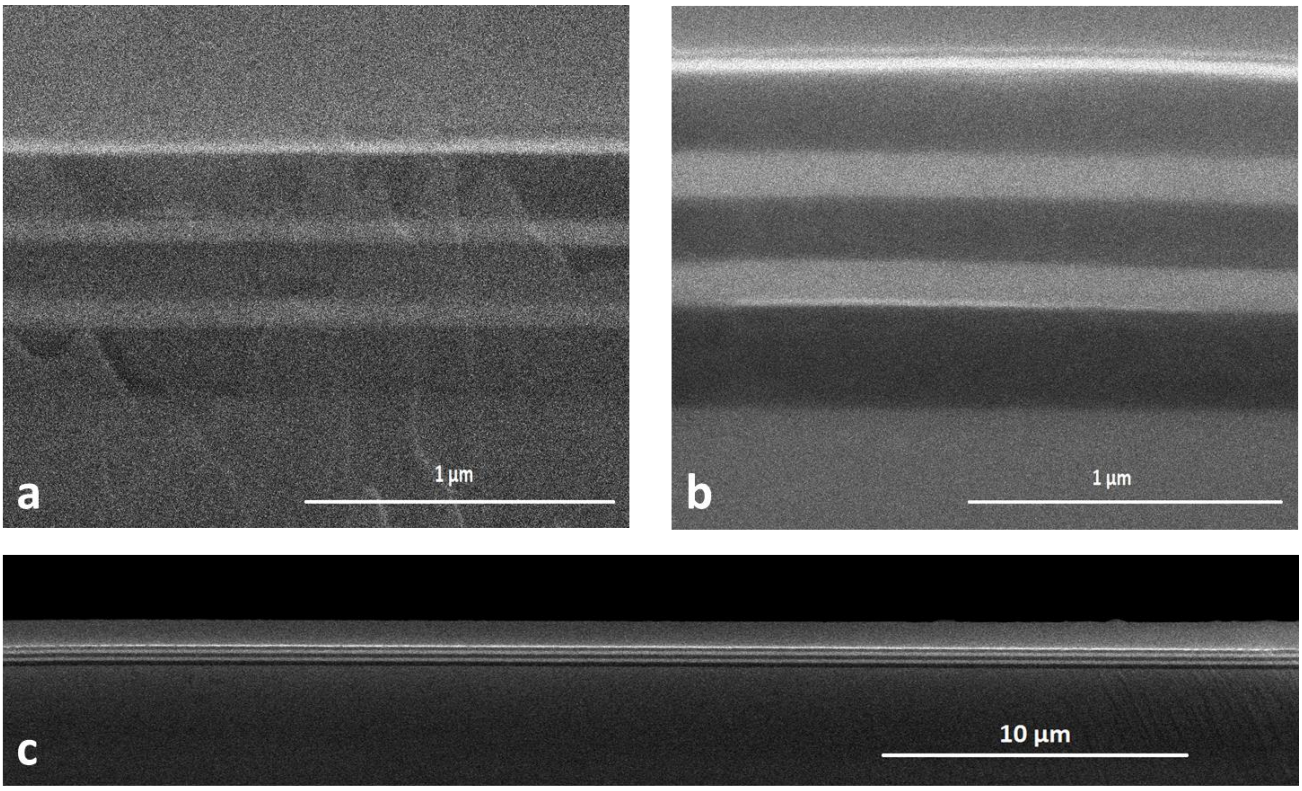

Figure 4. SEM images of cross sections of a five layered system, spin coated with 32.2 CuInX (a) and 64.4 mg ml^{-1} CuInX (b,c) deposited on a silicon wafer. The layer sequence in all images is (from bottom to top): silicon-cellulose-CIS-cellulose-CIS-cellulose-metal stripe.

It should be also mentioned that the cellulose and $CuInS_2$ layers exhibit good compatibility when it comes to the surface free energy (SFE, Fig. 5). The cellulose layers derived from CX exhibit a SFE of ca. 70 mN m^{-1} with a major disperse contribution to the total SFE, and a similar behavior is observed for the $CuInS_2$ surfaces (60 mN m^{-1}, with major disperse contributions). Only slight deviations for the different layers of each material are observed, which are probably caused by roughness contributions.

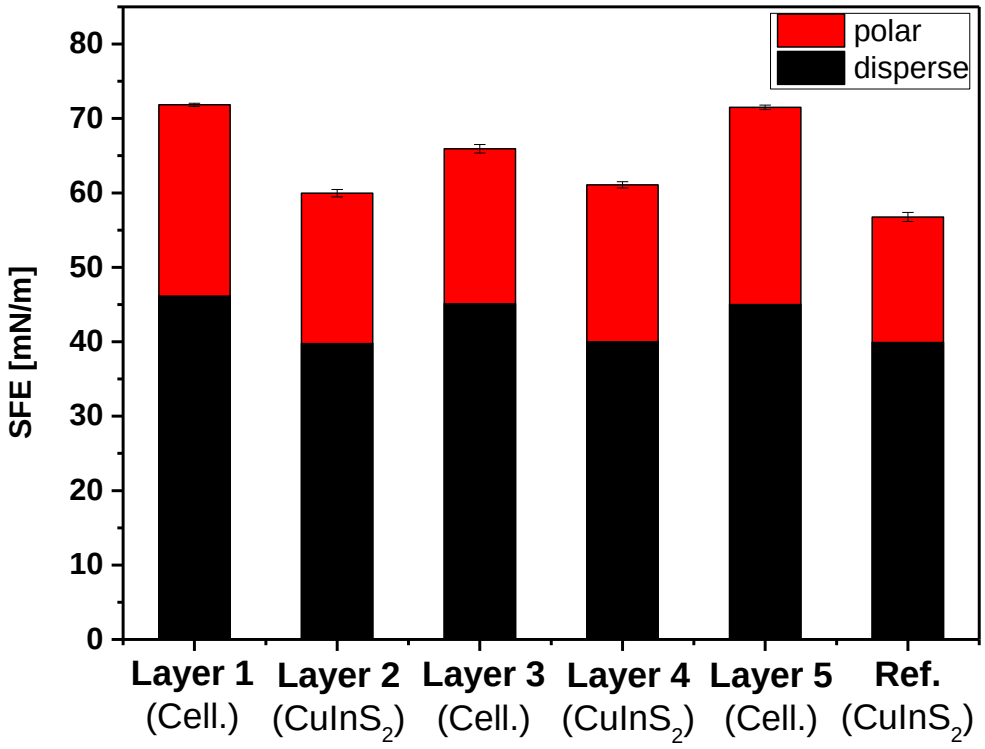

Figure 5. SFE values for every layer in the 5 layered system and a $CuInS_2$ reference thin film prepared on a silicon substrate. The CuInX concentration used for spin coating was 32.2 mg ml^{-1}.

3.4 Photo(electric) characterization

It is well known that $CuInS_2$ is an excellent semiconductor with a bandgap of 1.5 eV, absorbing in the visible (VIS) range of the electromagnetic spectrum. Figure 6 compares UV-Vis absorbance spectra in dependence of the number of deposited layers. These spectra have been obtained from the transmission and reflection spectra as described in the experimental section. The absorption onset for $CuInS_2$ nanoparticles is reported between 800 and 900 nm in literature, which fits well to the onset points visible in Fig. 6. (Rath et al., 2011; Reishofer, Rath, et al., 2017)

The cellulose layers are VIS transparent and did not absorb light in this wavelength region. Any absorption in the multilayer is therefore due to absorption of the $CuInS_2$ layers. According to the Lambert-Beer law, the intensity of the absorption is proportional to the layer thickness of the

films. Hence, a doubling of the layer thickness (when going from L2 to L4) results in a doubling of the absorption of the films. The significantly changed shape of the absorption spectrum of the multilayer stack after deposition of layer 5 originates from interference phenomena, which are also clearly observed in the reflection spectra of these films (Figure S8, supporting information).

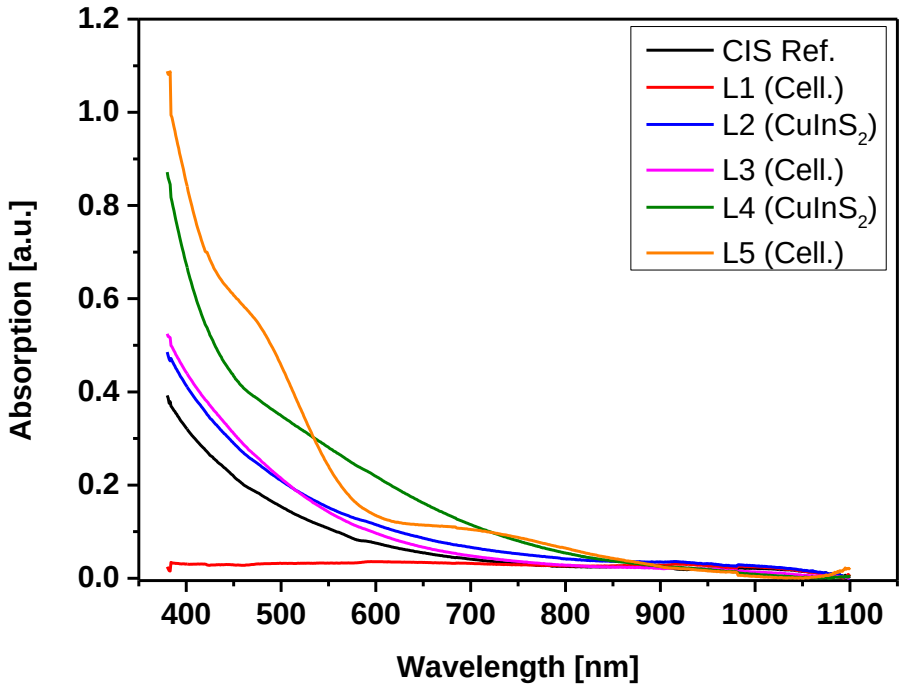

Figure 6. VIS absorption spectra of a cellulose $CuInS_2$ multilayer device with an increasing number of layers in the system having a final layer thickness of 560 nm and comparison to a $CuInS_2$ reference layer (40 nm). Thicknesses for the single layers are around 160 nm for cellulose and 40 nm for $CuInS_2$

Semiconducting layers separated by thin insulating films might find various technologically relevant applications. To electrically characterize the $CuInS_2$ thin films sandwiched between the cellulose layers, current/voltage curves of the $CuInS_2$ layers in different stages are shown in Fig. 7. The current/voltage curves show a linear characteristic due to the Ohmic nature of the contacts

to the $CuInS_2$ films. It can be clearly seen that the $CuInS_2$ layers are conductive and they also exhibited photoconductivity upon illumination. The two different layers consisting of $CuInS_2$ (i.e. L2 and L4) feature nearly the same current flow at a given potential and also the induced photocurrents are very similar. However, obviously the deposition of a top coating of cellulose onto these layers causes a drop in conductivity, which is observed for most of the samples. A possible reason for this could be the presence of microcracks, which could form due to the swelling of the cellulose film on top of the $CuInS_2$ film during the rinsing step to remove the NaTFAA salt formed during the regeneration of the cellulose xanthate. However, as the SEM images of the cross-sections revealed, the multilayer structure is intact and no indications of cracks throughout the whole layers were observed. Another issue in the determination of the currents is in the contacts to the $CuInS_2$ films. If the contact is exposed to the regeneration procedure, the electrode surface or the interface may be passivated leading to higher contact resistance. Moreover, the thicknesses of the $CuInS_2$ films are very low (only about 40-50 nm), which also explains the relatively low currents at a 10 mm distance between the electrodes.

To explore this further, the layer thickness of the $CuInS_2$ layers was increased by increasing of the CuInX concentration in the precursor solution. Additionally, these layers have then been compared to layers of similar thickness but obtained by consecutive spin coating steps of CuInX followed by immediate conversion to $CuInS_2$.

As mentioned above, a single $CuInS_2$ layer spin coated from the standard CuInX concentration (32.2 mg/mL) results in a layer thickness of approximately 40-45 nm. Each additional, subsequent spin coating of CuInX onto this layer leads to an increase of the thickness of another 40-45 nm, i.e. after two and three subsequent deposition and annealing steps, $CuInS_2$ layers with 90 and 140 nm thickness are obtained. When the CuInX concentration was increased (64.4 mg/mL), the $CuInS_2$ layer thickness was ca. 100, 200 and 300 nm, respectively. As can be seen in

Figure S10 a/b (supporting information), the deposition of a single $CuInS_2$ layer (100 nm) results in lower (photo-)conductivity than for a layer with the same thickness but deposited in several spin coating steps. Based on this observation it can be speculated that the $CuInS_2$ layers manufactured in several incremental steps are more capable to absorb the strain caused by the swelling cellulose during the rinsing thereby resulting in better electrical performance than the single deposited layers with the same thickness.

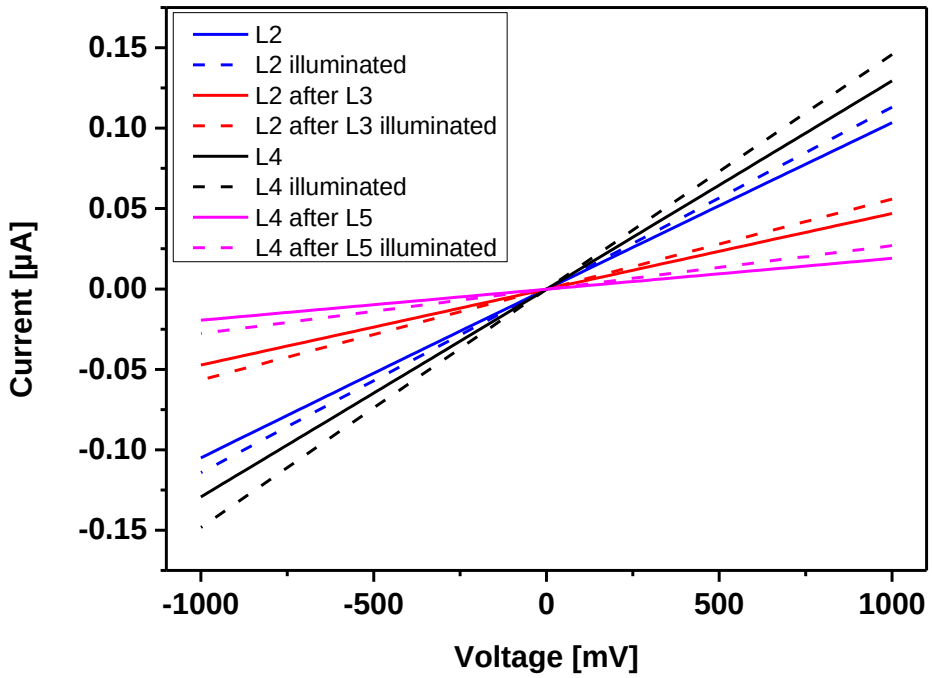

Figure 7. Current/voltage characteristics of the $CuInS_2$ layers after every layer spin coated on the system (CuInX concentration: 64.4 mg ml^{-1}).

3.5 Preparation of microstructured $CuInS_2$ thin films by UV-light illumination

In addition to hybrid and inorganic thin film solar cells, $CuInS_2$ layers are also applied in waveguides, sensors, photodetectors, electroluminescent devices or photo catalysts. In most of these applications microstructured films are required, which contain spatially confined patterns of the semiconductor. It has been reported that microstructures of $CuInS_2$ can be realized by

exposure of the copper and indium xanthate film to UV light.(T. Rath et al., 2013) During this process, the metal xanthate film acts as a negative resist, the CuInX film becomes insoluble by conversion to $CuInS_2$ in the UV exposed areas.

In the case of our multilayer system, metal masks have been positioned onto the CuInX films after spin coating followed by exposure to UV-light. After the UV treatment, the films were washed in chloroform, to remove the non-exposed areas. For the patterning, masks with varying geometry have been used each having a diameter of ca. 500 µm in diameter (see Figure S11). To prevent excessive exposure of the cellulose films to UV light, we chose a short exposure time with relatively low UV light intensity. This mild UV exposure enabled the patterning of the film, however, to improve the conductivity of the patterned $CuInS_2$ thin films, they were annealed after the development procedure in a second step. By the heating step at 170°C, the step height of the patterns decreased to values comparable to those observed for the conventionally heat treated films and also the obtained conductivities were comparable (see Figure 8).

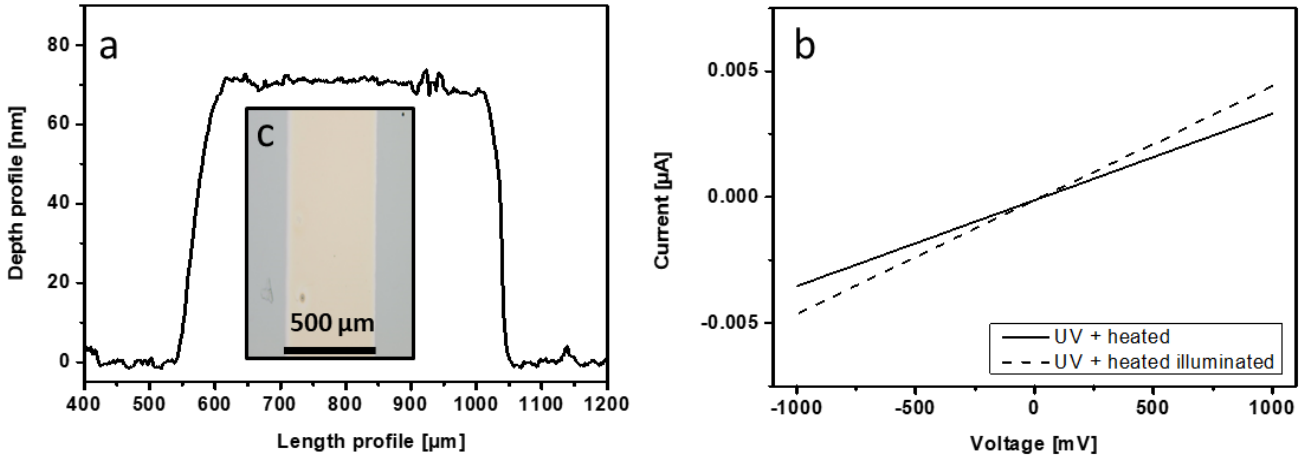

Figure 8. Microscopy image of a $CuInS_2$ stripe generated by UV exposure Step height of a $CuInS_2$ stripe generated by UV exposure determined by profilometry (a) and its current/voltage profile (b). Microscopy image of the $CuInS_2$ stripe on a silicon wafer (c).

4. Conclusion

We demonstrated a a proof of concept for the scalable manufacturing of cellulose-metal sulfide multilayered sandwich type films using cellulose xanthate precursors for the formation of cellulose and metal xanthate precursors for the formation of $CuInS_2$ layers. The approach uses subsequent spin coating steps to deposit the precursors onto a substrate (e.g., a silicon wafer) accompanied by a conversion in either cellulose (by TFA) or $CuInS_2$ (by heat). By variation of the concentration of the precursors, the film thickness can be easily varied for both of the components and homogeneous layers were obtained as shown by cross sectional analysis using SEM. The CuInX layers could also be converted to $CuInS_2$ using UV light, whereas the usage of masks allowed for the creation of $CuInS_2$ micropatterns with well-defined edges on the cellulose thin films. In principle, patterning at smaller scale is possible if masks with smaller feature sizes would be employed. The metal sulfide layers were conductive and photoconductivity was observed upon illumination. A 5 layered device could yield up to 0.05 µA at 1000 mV when the layer thickness of the $CuInS_2$ was set to 50 nm and the distance between the electrodes to 10 mm. The combination of CX as starting material for the development of cellulose thin films and CuInX as source for the inorganic $CuInS_2$ layers enables a fully solvent based process, in which every single layer could be produced via spin coating and the corresponding development of the layer. Cellulose as bottom, intermediate and top layer is a green, biodegradable, highly available and lightweight matrix while being an insulator for a conductive system. In addition, the presented approach is generic allowing for the generation of any metal sulfide from metal xanthate thereby opening many opportunities in different fields such as catalysis, thin film membranes and battery systems to mention just a few. Since CX, a major industrial product for viscose fibers and film manufacturing is used, the scalability of the approach into industrial

dimension is in principle possible. Although the subsequent spin-coating of different layers seems laborious, all the involved steps could be automatized in industry and the involved solution-based processing steps can be adapted to roll-to-roll compatible coating techniques. This includes the regeneration of CX to cellulose, rinsing as well as the heat treatment to convert the CuInX precursor to $CuInS_2$. It should be mentioned, that the recycling of the gaseous side products during the conversion of the xanthates is a well optimized process and does not pose major problems in industrial scale as already demonstrated for viscose manufacturing sites. However, the process still requires further optimization before upscaling can be taken into account. This involves a better understanding of the whole process involving probably *in situ* studies during the formation of the $CuInS_2$ layers at the cellulose-$CuInS_2$ interface as well as thorough investigations on the influence of the cellulose xanthate regeneration on the $CuInS_2$ layers underneath by grazing incidence small and wide angle scattering.

Acknowledgements

We kindly thank Martina Dienstleder (Graz Center for Electron Microscopy) for providing the schematic description of the ion beam slope cut technique and the Lenzing AG (Dr. Josef Innerlohinger) for supporting us with cellulose xanthate. WT and SE acknowledge financial support through the Accelerate3 project from the Interreg Vlaanderen-Nederland program and Flanders Innovation & Entrepreneurship for XPS. W.T. also thanks the Provincie West-Vlaanderen (Belgium) for financial support through his Provincial Chair in Advanced Materials.

References

Al-Shakban, M., Matthews, P. D., Zhong, X. L., Vitorica-Yrezabal, I., Raftery, J., Lewis, D. J., & O'Brien, P. (2018). On the phase control of CuInS2 nanoparticles from Cu-/In-xanthates. *Dalton Transactions,* 47(15), 5304-5309.

Andrews, D. A., Hurtubise, F. G., & Krassig, H. (1960). The Presence of Monothiocarbonate Substituents in Cellulose Xanthates. *Canadian Journal of Chemistry,* 38(8), 1381-1394.

Dautzenberg, H., & Philipp, B. (1970). Über Bildungsweise und Verhalten des Natriumdithiocarbonats. *Zeitschrift fur Anorganische und Allgemeine Chemie,* 375(2), 113-123.

Dunst, S., Rath, T., Radivo, A., Sovernigo, E., Tormen, M., Amenitsch, H., Marmiroli, B., Sartori, B., Reichmann, A., Knall, A.-C., & Trimmel, G. (2014). Nanoimprinted comb structures in a low bandgap polymer: thermal processing and their application in hybrid solar cells. *ACS Applied Materials & Interfaces,* 6, 7633-7642.

Filpponen, I., Kontturi, E., Nummelin, S., Rosilo, H., Kolehmainen, E., Ikkala, O., & Laine, J. (2012). Generic Method for Modular Surface Modification of Cellulosic Materials in Aqueous Medium by Sequential "Click" Reaction and Adsorption. *Biomacromolecules,* 13, 736−742.

Fradler, C., Rath, T., Dunst, S., Letofsky-Papst, I., Saf, R., Kunert, B., Hofer, F., Resel, R., & Trimmel, G. (2014). Flexible polymer/copper indium sulfide hybrid solar cells and modules based on the metal xanthate route and low temperature annealing. *Solar Energy Materials and Solar Cells,* 124, 117-125.

Kargl, R., Mohan, T., Koestler, S., Spirk, S., Doliska, A., Stana-Kleinschek, K., & Ribitsch, V. (2013). Functional Patterning of Biopolymer Thin Films Using Enzymes and Lithographic Methods. *Adv. Funct. Mater.,* 23(3), 308-315.

Kontturi, E., Tammelin, T., & Österberg, M. (2006). Cellulose model films and the fundamental approach. *Chemical Society Reviews,* 35, 1287-1304.

Kontturi, E., Thüne, P. C., & Niemantsverdriet, J. W. (2003). Cellulose Model Surfaces Simplified Preparation by Spin Coating and Characterization by X-ray Photoelectron Spectroscopy, Infrared Spectroscopy, and Atomic Force Microscopy. *Langmuir,* 19(14), 5735-5741.

Kontturi, K. S., Tammelin, T., Johansson, L.-S., & Stenius, P. (2008). Adsorption of Cationic Starch on Cellulose Studied by QCM-D. *Langmuir,* 24(9), 4743-4749.

Lai, C.-H., Lu, M.-Y., & Chen, L.-J. (2012). Metal sulfide nanostructures: synthesis, properties and applications in energy conversion and storage. *Journal of Materials Chemistry,* 22(1), 19-30.

MacLachlan, A. J., Rath, T., Cappel, U. B., Dowland, S. a., Amenitsch, H., Knall, A. C., Buchmaier, C., Trimmel, G., Nelson, J., & Haque, S. a. (2015). Polymer/nanocrystal hybrid solar cells: Influence of molecular precursor design on film nanomorphology, charge generation and device performance. *Advanced Functional Materials,* 25, 409-420.

Macreadie Lauren, K., Maynard-Casely Helen, E., Batten Stuart, R., Turner David, R., & Chesman Anthony, S. R. (2014). Soluble Xanthate Compounds for the Solution Deposition of Metal Sulfide Thin Films. *ChemPlusChem,* 80(1), 107-118.

Mikhlin, Y. L., Karacharov, A. A., & Likhatski, M. N. (2015). Effect of adsorption of butyl xanthate on galena, PbS, and HOPG surfaces as studied by atomic force microscopy and spectroscopy and XPS. *International Journal of Mineral Processing,* 144, 81-89.

Mohan, T., Spirk, S., Kargl, R., Doliska, A., Vesel, A., Salzmann, I., Resel, R., Ribitsch, V., & Stana-Kleinschek, K. (2012). Exploring the rearrangement of amorphous cellulose model thin films upon heat treatment. *Soft Matter*, 8, 9807-9815.

Mohan, T., Zarth, C., Doliska, A., Kargl, R., Grießer, T., Spirk, S., Heinze, T., & Stana-Kleinschek, K. (2013). Interactions of a cationic cellulose derivative with an ultrathin cellulose support. *Carbohydr. Polym.*, 92, 1046-1053.

Niegelhell, K., Süßenbacher, M., Jammernegg, K., Ganner, T., Schwendenwein, D., Schwab, H., Stelzer, F., Plank, H., & Spirk, S. (2016). Enzymes as Biodevelopers for Nano- and Micropatterned Bicomponent Biopolymer Thin Films. *Biomacromolecules*, 17(11), 3743-3749.

Ogura, K., & Sobue, H. (1968). Studies on the derivatives of sodium cellulose xanthate. Part I. Infrared absorption spectra and characteristic frequencies of C-S and C=S groups in sodium cellulose xanthate and its stable derivatives. *Journal of Polymer Science Part B: Polymer Letters*, 6(1), 63-67.

Orelma, H., Johansson, L.-S., Filpponen, I., Rojas, O. J., & Laine, J. (2012). Generic Method for Attaching Biomolecules via Avidin-Biotin Complexes Immobilized on Films of Regenerated and Nanofibrillar Cellulose. *Biomacromolecules*, 13, 2802-2810.

Owens, D. K., & Wendt, R. C. (1969). Estimation of the surface free energy of polymers. *Journal of Applied Polymer Science*, 13(8), 1741-1747.

Pradhan, N., Katz, B., & Efrima, S. (2003). Synthesis of High-Quality Metal Sulfide Nanoparticles from Alkyl Xanthate Single Precursors in Alkylamine Solvents. *The Journal of Physical Chemistry B*, 107(50), 13843-13854.

Rath, T., Edler, M., Haas, W., Fischereder, A., Moscher, S., Schenk, A., Trattnig, R., Sezen, M., Mauthner, G., Pein, A., Meischler, D., Bartl, K., Saf, R., Bansal, N., Haque, S. A., Hofer, F., List, E. J. W., & Trimmel, G. (2011). A Direct Route Towards Polymer/Copper Indium Sulfide Nanocomposite Solar Cells. *Advanced Energy Materials*, 1(6), 1046-1050.

Rath, T., Kaltenhauser, V., Haas, W., Reichmann, A., Hofer, F., & Trimmel, G. (2013). Solution-processed small molecule/copper indium sulfide hybrid solar cells. *Solar Energy Materials and Solar Cells*, 114, 38-42.

Rath, T., Padeste, C., Vockenhuber, M., Fradler, C., Edler, M., Reichmann, a., Letofsky-Papst, I., Hofer, F., Ekinci, Y., & Griesser, T. (2013). Direct extreme UV-lithographic conversion of metal xanthates into nanostructured metal sulfide layers for hybrid photovoltaics. *Journal of Materials Chemistry A*, 1, 11135-11140.

Redington, R. L., & Lin, K. C. (1971). Infrared spectra of trifluoroacetic acid and trifluoroacetic anhydride. *Spectrochimica Acta, Part A*, 27(12), 2445-2460.

Reishofer, D., Ehmann, H. M., Amenitsch, H., Gspan, C., Fischer, R., Plank, H., Trimmel, G., & Spirk, S. (2017). On the formation of Bi2S3-cellulose nanocomposite films from bismuth xanthates and trimethylsilyl-cellulose. *Carbohydrate Polymers*, 164, 294-300.

Reishofer, D., Rath, T., Ehmann, H. M., Gspan, C., Dunst, S., Amenitsch, H., Plank, H., Alonso, B., Belamie, E., Trimmel, G., & Spirk, S. (2017). Biobased Cellulosic–CuInS2 Nanocomposites for Optoelectronic Applications. *ACS Sustainable Chemistry & Engineering*, 5, 3115-3122.

Schaub, M., Wenz, G., Wegner, G., Stein, A., & Klemm, D. (1993). Ultrathin films of cellulose on silicon wafers. *Advanced Materials*, 5(12), 919-922.

Scheer, R., & Lewerenz, H. J. (1994). Photoemission study of evaporated CuInS2 thin films. II. Electronic surface structure. *Journal of Vacuum Science & Technology A*, 12(1), 56-60.

Široký, J., Blackburn, R. S., Bechtold, T., Taylor, J., & White, P. (2010). Attenuated total reflectance Fourier-transform Infrared spectroscopy analysis of crystallinity changes in lyocell following continuous treatment with sodium hydroxide. *Cellulose*, 17(1), 103-115.

Spirk, S., Belaj, F., Kahr, J., & Pietschnig, R. (2009). A one-dimensional coordination polymer formed by a 2:1 adduct of trifluoroacetic acid and its sodium salt. *Journal of Fluorine Chemistry*, 130(3), 365-367.

Vagvala, T. C., Pandey, S. S., Ogomi, Y., Ma, T., & Hayase, S. (2015). Investigation of metal xanthates as latent curing catalysts for epoxy resin via formation of in-situ metal sulfides. *Inorganica Chimica Acta*, 435, 292-298.

Weißl, M., Niegelhell, K., Reishofer, D., Zankel, A., Innerlohinger, J., & Spirk, S. (2018). Homogeneous cellulose thin films by regeneration of cellulose xanthate: properties and characterization. *Cellulose*, 25(1), 711-721.

Wolfberger, A., Petritz, A., Fian, A., Herka, J., Schmidt, V., Stadlober, B., Kargl, R., Spirk, S., & Griesser, T. (2015). Photolithographic patterning of cellulose: a versatile dual-tone photoresist for advanced applications. *Cellulose*, 22, 717-727.